

PCCP

Accepted Manuscript



This is an *Accepted Manuscript*, which has been through the Royal Society of Chemistry peer review process and has been accepted for publication.

Accepted Manuscripts are published online shortly after acceptance, before technical editing, formatting and proof reading. Using this free service, authors can make their results available to the community, in citable form, before we publish the edited article. We will replace this *Accepted Manuscript* with the edited and formatted *Advance Article* as soon as it is available.

You can find more information about *Accepted Manuscripts* in the [Information for Authors](#).

Please note that technical editing may introduce minor changes to the text and/or graphics, which may alter content. The journal's standard [Terms & Conditions](#) and the [Ethical guidelines](#) still apply. In no event shall the Royal Society of Chemistry be held responsible for any errors or omissions in this *Accepted Manuscript* or any consequences arising from the use of any information it contains.

Synthesis and thermodynamics of Ag–Cu nanoparticles

Simona Delsante^{1,2}, Gabriella Borzone^{1,2}, Rada Novakovic², Daniele Piazza¹, Giancarlo Pigozzi³,
Jolanta Janczak-Rusch³, Martina Pilloni⁴ and Guido Ennas⁴

¹Department of Chemistry and Industrial Chemistry, Genoa University and Genoa Research Unit of the National Consortium of Materials Science and Technology (INSTM), Via Dodecaneso 31, I-16146 Genoa, Italy

²National Research Council, Institute for Energetics and Interphases (CNR-IENI), Via De Marini 6, I-16149 Genoa, Italy

³Empa Swiss Federal Laboratories for Materials Science and Technology, Ueberlandstr. 129, 8600 Dübendorf, Switzerland

⁴University of Cagliari - Department of Chemical and Geological Science, Cagliari Research Unit of the National Consortium of Materials Science and Technology (INSTM) - Cittadella Universitaria di Monserrato, 09042 Monserrato (CA), Italy

E-mail: gabriella.borzone@unige.it

Keywords: Ag nanoparticles, Ag-Cu nanoparticles, melting temperature depression, nanoalloys, Differential Scanning Calorimetry

Abstract

Metallic silver, copper, and Ag-Cu nanoparticles (NPs) have been produced by chemical reduction method. The obtained nanoparticles were characterized by powder X-ray diffraction (XRD) and transmission electron microscopy (TEM). A side-segregated configuration was observed for the one-pot synthesized Ag-Cu NPs, and the melting temperature depression of about 14 °C was found by differential scanning calorimetry (DSC). A comparison between the new experimental data, the literature data on Ag-Cu bimetallic NPs and the corresponding theoretical values obtained from the Ag-Cu nano-sized phase diagram was done, whereas the melting behaviour of Ag and Cu metal nanoparticles was discussed in the framework of the liquid layer model (LLM).

1 Introduction

Metallic and bimetallic nanoparticles (NPs) possess unique properties which can provide solutions to engineering problems that cannot be solved with conventional alloyed metals; for this reason they have been considered for a variety of applications. The chemistry of nanoalloys has been widely investigated to be employed in catalysis, photonics and electronic devices, among many others listed in.¹⁻⁵ Recently, the advances in the synthesis procedures and the main applications of metallic

nanoalloys have been reviewed.⁶ The main methods employed for the synthesis use microwave (i.e. microwave heating, microwave plasma treatment, microwave-assisted solvothermal technique), molecular/ion/atom beams (cluster formation via gas aggregation, via laser-assisted synthesis, laser ablation), chemical vapour deposition, electrochemical synthesis, thermal decompositions and chemical reduction.

Among the processing routes mentioned above, the chemical reduction technique is one of the most suitable due to its simplicity and because it can assure the sample preparation on a multigram scale.⁷ Furthermore, it has been found to be the most convenient for industrial manufacture; in fact it is a comparatively inexpensive and easy way to produce nanoparticles.

It is well known that the large surface/volume ratio in small or nanosized particle systems has significant effects on their thermodynamic properties and phase relations, and NPs have the melting temperatures lower than their bulk counterparts. Pawlow⁸ in 1909 postulated that the melting point depression is due to the large influence of the surface energy on the energetics and structure of small particles. After fifty years, the experimental validation has been firstly done on thin films of Sn, Pb and Bi studied at various temperatures by electron diffraction method and reported by Takagi.⁹ Subsequently Buffat and Borel calculated the size of Au particles using the data obtained by a scanning electron diffraction technique and determined their melting temperature depression by observing the disappearance of electron diffraction patterns.¹⁰ By transmission electron microscope (TEM) Coombes¹¹ determined the melting temperature depression of about 200 °C for Pb nanoparticles with a radius of 3 nm. More recently Zhang et al.¹² observed a significant melting point depression for 0.1-10 nm thick discontinuous indium layers. The phenomenon of the melting point depression in nano-layered brazing fillers has been observed experimentally by Janczak-Rusch et al.¹³ Similarly, the melting temperature depression of Sn-based nanoalloys synthesized via various techniques has also been regarded as a promising property for applications in electronics.¹⁴⁻

16

Since the pioneer work of Pawlow⁸, different theoretical models describing the dependence of melting point on particle size have been assessed and during the years, these models have been further experimentally verified by many authors that studied the melting behaviour of various metallic nanoparticles and, using own experimental data, new models have also been developed.^{10,17-20} Recently, Barybin and Shapovalov²¹ reviewed the thermodynamic models available in literature related to the melting temperature depression of nanosized metal particles. The experimental validation of those semi empirical laws has been mainly done by using the corresponding experimental data on Sn, Bi, Au, Pb and In.^{7, 9-12, 21.}

As far as the melting temperature depression of binary alloys is concerned, the CALPHAD (CALculation of PHase Diagrams) approach²² has been extended to calculate nano-sized phase diagrams taking into account the effect of surface energy on the thermodynamic properties of small systems.²³ In order to study the melting behaviour of pure metals and alloys at nano-scale, a model describing the melting temperature depression as a function of particle size was combined with the CALPHAD method and applied to the Bi-Pb²⁴ and the Ag-Sn²⁵ nano-sized systems. The Ag-Cu system has been considered suitable as a model because its binary phase diagram shows a simple eutectic reaction (L (39 at.% Cu) \leftrightarrow (Ag) + (Cu)) that takes place at 780 °C.²⁶ The aim of our investigation has been to synthesize naked Ag, Cu and bimetallic Ag-Cu nanoparticles by a low temperature chemical reduction method and to analyse their melting behaviour by using a sensitive differential scanning calorimeter (DSC) in order to correlate the particle size with its melting temperature. Based on the aforementioned combined approach, the new experimental results obtained have been analyzed in the framework of the CALPHAD method used to calculate the Ag-Cu nano-sized phase diagram²⁷ and subsequently compared to the corresponding literature data.²⁸ DSC data can be very useful for the validation of the theoretically predicted nano-sized phase diagrams as well as of the corresponding models describing the melting behaviour of bimetallic NPs.

2 Experimental section

2.1 Chemicals and synthesis

The objective of our research was to synthesize both pure metallic Ag and Cu NPs and bimetallic Ag-Cu eutectic nanoalloys by a low temperature chemical reduction method in aqueous solution. Ag NPs were prepared by using Ag_2SO_4 (Alfa Aesar, 99,999 mass %; 0.05M or 0.01M) as a precursor and KBH_4 (Alfa Aesar, 98 mass %; 0.05 M or 0.01 M) as a reducing agent. Cu nanoparticles were synthesized according to the procedure described in^{29,30} by using $\text{CuSO}_4 \cdot 6\text{H}_2\text{O}$ (Panreac, 99,993 mass %; 0.02 M), Polyethylene glycol (PEG6000, Alfa Aesar; in large excess as capping agent), L-(+)-ascorbic acid (Alfa Aesar 99+ %, 0.02 M as antioxidant agent) and NaBH_4 or KBH_4 (0.02M, as reducing agent). As for the Ag-Cu nanoparticles, the same precursors have been employed (Ag_2SO_4 and $\text{CuSO}_4 \cdot 6\text{H}_2\text{O}$) in a ratio which allowed to achieve the eutectic Ag-39Cu (at %) composition using KBH_4 as reducing agent and PEG6000 as capping agent. Bidistilled water was purged with argon prior to use.

All synthesis were carried out under argon atmosphere in a five-neck round-bottom flask (1000 ml) equipped with a dropping funnel; the salt solutions were added dropwise to a solution containing borohydride and PEG6000 (except for Ag) which was vigorously stirred while maintained

approximately at 0 °C with an ice bath for around 30 minutes before the salt addition. The reaction time after the end of the salt addition was optimized to be 20 min for Ag NPs and 60 min for Cu and Ag-Cu NPs. The resulting fine precipitate was filtered under argon and washed first with distilled water and then with acetone in order to remove the unreacted reagents. The recovered powders were dried under flowing argon for 12 h. All steps of the synthesis (reaction, washing and drying) were carried out in argon atmosphere and its flux was checked and controlled in order to repeat the synthesis in the same conditions. At the end of the synthesis, the dried powders were passivated by air oxygen.

2.2 Characterization

X-ray powder diffraction (XRD) and Transmission Electron Microscopy coupled with Energy Dispersive Spectroscopy (TEM/EDS) were used to determine the crystalline nature of the samples, the size and the composition of the particles. The XRD analysis was performed using a Philips X'Pert MPD machine (Philips, Almelo, The Netherlands) equipped with a copper target, excited to 40 kV and 30 mA, and a solid state detector; the HR-TEM analysis was performed using a JEOL JEM 2200FS TEM, operating at 200 kV equipped with a field emission source, an OmegaVR energy filter, EDX, and HAADF detectors. The thermal behaviour of the samples has been investigated by a heat flux Differential Scanning Calorimetry (DSC) using a DSC111 SETARAM apparatus designed as a Calvet calorimeter. The calorimeter was calibrated by measuring the melting temperature of metallic In, Sn, Pb and Zn (99.999 mass % purity) and the temperature was obtained with an accuracy of ± 0.5 °C. The NPs were inserted in a sealed Ta crucible and then subjected to a thermal cycle from 25 to 800 °C and back at a heating/cooling rate of 5 °/min.

The onset temperature of the thermal effect on heating was selected as the temperature of the occurring transformation. Indeed, only the effects observed on heating are significant for the thermal behaviour of the nanoparticles because the cooling effects are related to the solidification of the bulk material, as commented later in Section 3.

In order to check the status of the samples after the DSC analysis, a Scanning Electron Microscope (SEM, Zeiss EVO 40) was employed by using a backscattered electron detector (BSE) to reveal the compositional contrast between the different phases and a Secondary Electron Detector (SE) to evaluate their morphology. Quantitative Electron-Probe Microanalysis (EPMA) data were collected at 20 kV on a Link system Ltd. Instrument equipped with an Energy Dispersive Spectroscopy (EDS) detector. A counting time of 100 s and a ZAF correction program were adopted. Certified pure elements were used as reference standards, while cobalt was adopted for calibration purposes.

The software package Inca Energy (Oxford Instruments, Analytical Ltd., Bucks, U.K.) was employed to process X-ray spectra.

2.3 The Ag-Cu nano-sized system: CALPHAD method and LLM thermodynamic model

The aforementioned thermodynamic models that describe the melting behaviour of metal nanoparticles are relatively simple nonlinear equations that involve the quantities such as the thermodynamic functions on the mixing or formation, bulk melting temperature, pressure, particle size, molar volume or density, interfacial tensions between the solid-liquid, liquid-vapour and solid-vapour of a system.²¹ Some of the models contain adjustable parameters that were calculated from available experimental data by means of the best fit, providing a good agreement between theoretical and experimental curves for the systems investigated.^{17-19,21} The models cited in the literature²¹ and their experimental validation on pure metal nanoparticles indicate that the melting temperature depression and particle size are inversely proportional. In the present work the melting behaviour of Ag and Cu NPs has been predicted by the liquid layer model (LLM).³¹ The melting temperature depression is given by

$$\frac{\Delta T_m(r)}{T_m^{bulk}} = \frac{2v_s \cdot \sigma_{sl}}{\Delta H_m \cdot r} \left[1 + \frac{r \cdot \sigma_l}{(r+l)\sigma_{sl}} \left(1 - \frac{v_l}{v_s} \right) \right] \quad (1)$$

where $\Delta T_m(r) = T_m^{bulk} - T_m^{NPs}$, ΔH_m is the molar heat of fusion, v_s and v_l are the molar volume of the solid and liquid, respectively. σ_s , σ_s and σ_{sl} are the interfacial energies of the solid-gas, liquid-gas and solid-liquid, respectively, and l is the critical thickness of the liquid layer.

Taking into account the effect of surface energy on the total Gibbs free energy of small systems, Tanaka and Hara²³ extended the CALPHAD method²² to calculate phase diagrams of simple binary nanosized systems, characterised by lens type or eutectic phase diagrams. It has also been shown that the method is appropriate for binary nanosized systems with the lowest particle size limit of 4-5 nm.^{23,24}

3 Results and discussion

Four samples of Ag NPs (Ag01, Ag02, Ag03 and Ag04) were prepared and characterized by XRD and TEM/EDS and then subjected to a thermal cycle from 25 to 800 °C with the DSC at a scanning rate of 5 °/min. After the DSC analysis, the state of the samples was checked by SEM/EDS and XRD analysis. The XRD patterns of the anhydrous as-prepared Ag particles showed the presence of only the cubic Ag (cF4–Cu) phase whereas the TEM investigation pointed out the great tendency of

the NPs to agglomerate and confirmed the absence of oxides. The average dimension of the particles was calculated to be around 15 ± 20 nm by using the Scherrer formula³² and evaluated from the TEM images. The synthesis procedure is quite reproducible. See Fig. 1 for a comparison of the XRD patterns of the Ag NPs samples (sample #Ag01 *Vs.* sample #Ag02) and Fig. 2 for the TEM image of sample #Ag02. The TEM image displays that agglomeration takes place as a result of nanoparticle interaction giving the grey contrast; no impurities were detected by EDS analysis. Some samples were subjected to DSC analysis in order to check their behaviour during the heating and their morphology after this treatment. The DSC heating curve shows a fluctuation in the temperature range 600-750 °C which can be ascribed to the coalescence process (Fig. 3a, sample #Ag02) and the SEM image confirmed the growth of the particles (Fig. 3b, sample #Ag02). The melting point has not been detected due to the operational limit of the instrument (around 800 °C). As described in,^{28,30,33} due to a strong tendency of copper to oxidation, the synthesis of Cu NPs has been much more difficult with respect to that of Ag NPs. Indeed, Cu NPs obtained were surrounded by a layer of copper oxide and the average dimension ranging within 10 ± 15 nm, by using the Scherrer formula³² and the elaboration of the TEM images.

Table 1 summarizes the Ag-Cu NPs samples synthesized near to the eutectic composition (~ 39 at % Cu) by reducing an aqueous solution of Ag_2SO_4 and $\text{CuSO}_4 \cdot 6\text{H}_2\text{O}$ with KBH_4 and PEG6000. The XRD patterns of the as-prepared specimens show the presence of Ag (*cF4*-Cu), Cu (*cF4*-Cu) and Cu_2O (*cP6*- Cu_2O) as displayed in Fig. 4 for sample #AgCu08. The dominant peaks at $2\theta \sim 38^\circ$, 44° , 64° , 78° are assigned to the cubic metallic Ag (see Miller index assigned to the peaks) and next to the Ag peak at $2\theta \sim 43^\circ$ there is the only visible peak which identify the presence of Cu; a faint peak at $2\theta \sim 37^\circ$ (not clearly visible in the figure) revealed the presence of Cu_2O . The average NPs dimension of 10 ± 15 nm was calculated by using the Scherrer formula. TEM images show that particles were agglomerated; nevertheless, the particles size distribution seems to be centred on 15 nm. Aside of the main particles population a second population of ~ 2 nm NPs is also visible (see Fig. 5, sample #AgCu08). Based on the aforementioned data analysis of the NPs samples there is the size distribution around 10-15 nm for the main population and NPs of that size have been considered as representative, also taking into account that, a whole quantity of 20-30 mg NPs prepared for the present study, have been used to perform DSC measurements.

Different arrangements of the two elements in bimetallic nanoclusters have been described in literature, namely: core-shell, sub-cluster segregated (Janus), mixed, three shells, as reported in.^{1,34} Usually when small nanoclusters have a very favorable surface/volume ratio the core-shell structure is expected to be formed, where the core of a metal A is covered by thin shell (possibly a monolayer) of a metal B.^{35,36} The core-shell structure has been experimentally observed for the Bi-

Sn eutectic nanoalloy and was reported by the present authors.⁷ In the case of Ag-Cu nanoparticles, copper cores covered by silver shells can be expected.³⁷ Nevertheless, the EDX mapping showed that Ag and Cu adopted a “side-segregated” configuration with Cu nanoparticles linked on Ag and a consistent amount of oxygen was observed on Cu particle surface (see Fig. 6, sample #AgCu09). These observations are in agreement with the experimental results obtained by EFTEM for the chemical configuration of Ag-Cu bimetallic NPs synthesized by a physical route.³⁸ The influence of Cu₂O on the NPs configuration was also highlighted.

After characterization, the synthesized Ag-Cu NPs were inserted in a sealed Ta crucible and analyzed by DSC at a heating and cooling rate of 5 °/min. The onset temperatures measured for the Ag-Cu NPs are listed in Table 1 and a good reproducibility can be observed. We should underline that, after the DSC analysis, solidified samples cannot be considered anymore NPs but bulk materials. A typical heating/cooling curve obtained is displayed in Fig. 7 (sample #AgCu05). The endothermic peak registered on heating having an onset point at $T = 766$ °C can be ascribed to the eutectic reaction $L \leftrightarrow (Ag) + (Cu)$; this indicates the melting point depression of about 14 °C. The exothermic peak at 775 °C, visible on cooling is related to the solidification of the Ag-Cu bulk alloy with a slight undercooling. The undercooling effect occurring in bulk materials is well known and it is described in.³⁹

We often observed a fluctuation in the signal before the melting process that could be related to the coalescence process; see by analogy the DSC curve of Ag NPs in Fig. 3a. It has been considered noteworthy to compare the behaviour to thermal treatment of the “side-segregated” NPs obtained by “one-pot synthesis” with that of a “mechanical mixture” of Ag NPs and Cu NPs (surrounded by an oxide layer).³⁰ To this end, a DSC measurement was performed under the same experimental conditions on Ag and Cu NPs “mixed” in an Ag/Cu ratio corresponding to the eutectic composition. As can be seen in Fig. 8, the “mechanical mixture” of Ag + Cu NPs has a very similar thermal behaviour in comparison with the one-pot synthesized Ag-Cu NPs samples. The melting point depression is lower (10 °C), but still present ($T_{\text{onset}} = 770$ °C on heating), and the crystallization exothermic peak has the same onset temperature (775 °C) which corresponds to the solidification of the eutectic bulk alloy with a slight undercooling.

However, the relatively low melting point depression observed for the NPs, may be ascribed either to the lowering of the eutectic temperature of Ag-Cu nanosized system with respect to the bulk alloy ($L \leftrightarrow (Ag) + (Cu)$, $T = 780$ °C) or to the presence of Cu₂O formed during the processing route. The combined effects of the two phenomena may be also possible, as it has been observed in the case of Cu nanoparticles.^{28,33} After DSC, the SEM/EPMA and XRD analyses showed for both

the Ag-Cu NPs samples and for the “mechanical mixture” of “Ag + Cu” NPs the typical binary eutectic morphology (Fig. 9a and 9b) peculiar for the bulk material.

Until now thermal data on the melting temperature depression experimentally obtained on naked Ag-Cu NPs have never been published. The only experimental data on the melting temperature depression of the Ag-Cu eutectic nanoalloy, synthesized “in carbon shells”, are those reported by Huang et al.²⁸ For nanosized eutectic alloy with a particle size of 10 nm those authors observed a decrease of 75 °C with respect to the melting temperature of its bulk counterpart ($T_e=780$ °C).²⁶ The melting temperature depression of the eutectic Ag-Cu nanoalloy obtained in the present work differs up to 60 °C from the data reported in²⁸ due to different processing routes of nanoparticles synthesis. The nanosized Ag-Cu phase diagram has been firstly calculated by Hajra and Acharya.⁴⁰ These authors studied the melting temperature depression of the Ag-Cu for nanoparticles of 1 and 5 nm and reported the predicted melting temperatures only for nanoparticles of 1 nm. Keeping in mind that the CALPHAD approach has been successfully applied to calculate the phase diagrams of binary nanosized systems with the lower limit of particle size about 4-5 nm,^{23,24,41} the theoretical results⁴⁰ were not considered here. Garzel et al.²⁷ have assessed the nanosized Ag-Cu phase diagram and for the eutectic Ag-Cu nanoalloy the melting temperature depression of 10-180 °C was found. Taking into account the melting temperature depression of the Ag-Cu eutectic nanoalloy calculated by the CALPHAD method²⁷ and combining those results with the LLM model (Eq.(1)), its melting behaviour was predicted for bimetallic NPs ranging between 10 and 35 nm. The experimental results obtained in the present work, the literature data²⁸ and the LLM-curve describing melting of eutectic Ag-Cu NPs are shown in Fig. 10. The new experimental data obtained in the present work and the corresponding values calculated by the CALPHAD method²⁷ differ up to 20 %. The relationship $\Delta T_m \propto r^{-1}$ is available for both, metal and bimetallic nanoparticles.^{17,24} A linear dependence of the melting temperature depression observed in the case of Ag-Cu eutectic bimetallic nanoparticles (Fig. 11), substantiates the melting curve predicted by the CALPHAD method combined with the LLM model.^{27,31} In order to analyze the melting behaviour of the Ag-Cu nanosized system, the melting temperature depression of Ag and Cu metal nanoparticles, calculated by the LLM together with corresponding literature data^{28,42-44} are also shown (Fig. 10).

4 Concluding remarks

The thermodynamics of solid-liquid phase equilibria in the Ag-Cu nanosized system has been studied and the experimental verification of the melting temperature depression of Ag-Cu eutectic nanoparticles (< 50 nm) was obtained by using a sensitive differential scanning calorimeter. Cu, Ag and Ag-Cu anhydrous nanosized particles were successfully synthesized by cost-effective chemical

reduction method. Composition and morphology of the nanoalloys were characterized by XRD, TEM and DSC analyses. The results obtained make it possible to perform an experimental validation of semi empirical models related to the melting temperature depression of bimetallic nanoalloy particles. In this work a melting point depression in the range of 10-14°C was observed both for the one-pot synthesized Ag-Cu NPs and for a “Ag + Cu mechanical mixture” of NPs, which are comparable to the corresponding results calculated by the CALPHAD method.

Acknowledgments

This research is a contribution to the European COST Action MP0903 “Nanoalloys as advanced materials: from structure to properties and applications”.

References

- 1 R. Ferrando, J. Jellinek and R.L. Johnston, *Chem. Rev.*, 2008, **108**, 847.
- 2 *Nanoparticles. From Theory to Application*, ed. G. Schmid, Wiley-VCH Verlag GmbH & Co. KGaA, Weinheim, 2004.
- 3 R.K. Roy, S.J. Kernion, S. Shen and M.E. McHenry, *Appl. Phys. Lett.*, 2011, **99**, 192506.
- 4 R.K. Roy, S. Shen, S.J. Kernion and M.E. McHenry, *J. Appl. Phys.*, 2012, **111**, 07A301.
- 5 F. Calvo, *Phys. Chem. Chem. Phys.*, 2015, DOI: 10.1039/c5cp00274e
- 6 B.M. Munoz-Flores, B.I. Kharisov, V.M. Jimenez-Perez, P. Elizondo Martínez and S.T. Lopez, *Ind. Eng. Chem. Res.*, 2011, **50**, 7705.
- 7 F. Frongia, M. Pilloni, A. Scano, A. Ardu, C. Cannas, A. Musinu, G. Borzone, S. Delsante, R. Novakovic and G. Ennas, *J. Alloys Compd.*, 2015, **623**, 7.
- 8 P. Pawlow, *Z. Phys. Chem.*, 1909, **65**, 545.
- 9 M. Takagi, *J. Phys. Soc. Jpn.*, 1954, **9**, 359.
- 10 Ph. Buffat and J-P. Borel, *Phys. Rev. A*, 1976, **13**, 2287.
- 11 C. J. Coombes, *J. Phys. F: Metal Phys.*, 1972, **2**, 441.
- 12 M. Zhang, M. Yu. Efremov, F. Schiettekatte, E. A. Olson, A. T. Kwan, S. L. Lai, T. Wisleder, J.E. Green and L. H. Allen, *Phys. Rev., B*, 2000, **62**, 10548.
- 13 J. Janczak-Rusch, G. Pigozzi, B. Lehmert, M. Parlinska, V. Bissig, W. Tillmann, L. Wojarski and F. Hoffmann, Deposition and utilization of nano-multilayered brazing filler systems designed for melting point depression, in: *Brazing and Soldering 2012*, IBSC Proceedings of 5th Intl. Conference, 2012.
- 14 J. Yan, G. Zou, A. Wu, J. Ren, A. Hu and Y.N. Zhou, *J. Electronic Mater.*, 2012, **41**, 1886.
- 15 H. Jiang, K. Moon and C.P. Wong, *Microelectron. Reliab.*, 2013, **53**, 1968.

- 16 J. Yan, G. Zou, Y. Zhang, J. Li, L. Liu, A. Wu and Y.N. Zhou, *Mater. Trans.*, 2013, **54**, 879.
- 17 C.R.M. Wronski, *Brit. J. Appl. Phys.*, 1967, **18**, 1731.
- 18 P.R. Couchman and W.A. Jesser, *Nature*, 1977, **269**, 481.
- 19 S.L. Lai, J.Y. Guo, V. Petrova, G. Ramanath and L.H. Allen, *Phys. Rev. Lett.*, 1996, **77**, 99.
- 20 C. Zou, Y. Gao, B. Yang and Q. Zhai, *Trans. Nonferrous Met. Soc. China*, 2010, **20**, 248.
- 21 A. Barybin and V. Shapovalov, *J. Appl. Phys.*, 2011, **109**, 1.
- 22 N. Saunders and A.P. Miodownik, *CALPHAD (Calculation of Phase Diagrams): A Comprehensive Guide*, Exeter, Pergamon; 1998.
- 23 T. Tanaka and S. Hara, *Z. Metallkd.*, 2001, **92**, 467.
- 24 W.A. Jesser, R.Z. Shneck and W.W. Gile, *Phys. Rev.*, 2004, **B 69**, 144121.
- 25 J. Sopoušek, J. Vřešťál, A. Zemanova and J. Bursik, *J. Min. Metall. Sect. B-Metall.*, 2012, **48**, 419.
- 26 T.B. Massalski in Binary Alloy Phase Diagram, ASM International, T.B. Massalski Ed. in chief, Materials Park Ohio, 2nd edition, 1990, vol.1, pp. 28-29.
- 27 G. Garzel, J. Janczak-Rusch and L. Zabdyr, *Comput. Coupling Phase Diagrams Thermochem.*, 2012, **36**, 52.
- 28 C.H. Huang, H.P. Wang, J.E. Chang and E.M. Eyring, *Chem. Commun*, 2009, **31**, 4663.
- 29 T.M.D. Dang, T.T.T. Le, E. Fribourg-Blanc and M.C. Dang, *Adv. Nat. Sci.: Nanosci. Nanotechnol.*, 2011, **2**, 015009.
- 30 “Synthesis, characterization and thermal stability of Cu nanoparticles“, S. Delsante, R. Novakovic and G. Borzone, in preparation.
- 31 H. Reiss and I.B. Wilson, *J. Colloid Sci.*, 1948, **3**, 551.
- 32 A. L. Patterson, *Phys. Rev.*, 1939, **56**, 978.
- 33 O.A. Yeshchenko and I.M. Dmytruk, *Phys. Rev. B*, 2007, **75**, 1.
- 34 H. Peng, W. Qi, S. Li and W. Ji, *J. Phys. Chem. C*, 2015, **119**, 2186.
- 35 M. Cazayous, C. Langlois, T. Oikawa, C. Ricolleau and A. Sacuto, *Phys. Rev. B*, 2006, **73**, 113402.
- 36 R.G. Chaudhuri and S. Paria, *Chem. Rev.*, 2012, **112**, 2373.
- 37 F. Baletto, C. Mottet and R. Ferrando, *Phys. Rev. B*, 2002, **66**, 155420.
- 38 C. Langlois, Z.L. Li, J. Yuan, D. Alloyeau, J. Nelayah, D. Bochicchio, R. Ferrando and C. Ricolleau, *Nanoscale*, 2012, **4**, 3381.
- 39 W.J. Boettinger, U.R. Kattner, K.-W. Moon and J. H. Perepezko in NIST Recommended Practice Guide spec. pub. 960-15, DTA and Heat-Flux DSC Measurements of Alloy Melting and Freezing, 2006.

40 J.P. Hajra and S. Acharya, *J. Nanosci. & Nanotechn.*, 2004, **4**, 899.

41 J. Park and J. Lee, *Comput. Coupling Phase Diagrams Thermochem.*, 2008, **32**, 135.

42 T. Castro and R. Reifenger, *Phys. Rev. B*, 1990, **42**, 8548.

43 W. Hu, S. Xiao, H. Deng, W. Luo and L. Deng in *Thermodynamic Properties of Nano-Silver and Alloy Particles, Silver Nanoparticles*, D. Pozo Perez Ed., Ch. 1, 2010.

Online: <http://www.intechopen.com/books/silver-nanoparticles/thermodynamic-properties-of-nano-silver-and-alloy-particles>

44 J.G. Lee, J. Lee, T. Tanaka and H. Mori, *Phys. Rev. Lett.*, 2006, **96**, 075504.

Table 1 Summary of the prepared samples: mean size dimension and DSC thermal effects. The onset temperature of the thermal effect on heating corresponds to the occurring transformation (melting temperature of the NPs); the cooling effects are related to the solidification of the bulk material (see text).

Batch #	Mean size dimension [nm]	Onset DSC signal Heating/Cooling [°C]
AgCu01	10-15	n.m
AgCu02	Aborted	
AgCu03	10-15	n.m
AgCu04	10-15	n.m
AgCu05	10-15	766 / 775
AgCu06	Aborted	
AgCu07	10-15	768 / 775
AgCu08	10-15	768 / 770
AgCu09	10-15	766 / 775
AgCu10	10-15	766 / 770
AgCu11	10-15	766 / 775
AgCu12	Aborted	
AgCu13	10-15	766 / 773
AgCu14	10-15	766 / 774
AgCu15	10-15	766 / 773
AgCu16	10-15	764 / 775
AgCu17	Aborted	

n.m = not measured

Figure captions

Fig. 1 XRD pattern of the as-prepared Ag NPs sample #Ag01 (solid line) *Vs.* sample #Ag02 (dotted line). The diffraction peaks belongs to the cubic $cF4$ -Cu phase (Miller Index are also inserted).

Fig. 2 TEM image of the as-prepared Ag NPs sample #Ag02 (see text).

Fig. 3 DSC curve on heating (Fig. 3a) the Ag NPs sample #Ag02 and SEM/SE aspect of the same sample after DSC analysis (Fig. 3b).

Fig. 4 XRD pattern of the as-prepared Ag-Cu NPs sample #AgCu08. The peaks of the cubic ($cF4$ -Cu) Ag phase are indicated by the asterisk and the Miller index are reported; the open circle indicates the only visible peak of the cubic ($cF4$ -Cu) Cu phase.

Fig. 5 TEM (left side) and HRTEM (right side) images of the Ag-Cu NPs sample #AgCu08.

Fig. 6 TEM/EDX mapping of the Ag-Cu NPs sample #AgCu09 (silver = blue; copper = red-orange; oxygen = green).

Fig. 7 DSC curve heating (solid line)/cooling (dotted line) for NPs sample #AgCu05 registered at 5 °/min. The onset point on heating (766 °C) and on cooling (775 °C) are indicated.

Fig. 8 DSC curve heating (solid line)/cooling (dotted line) for the “mixed” Ag and Cu NPs at the eutectic Ag/Cu ratio. The onset point on heating (770 °C) and on cooling (775 °C) are indicated.

Fig. 9 Comparison between the SEM/BSE image of sample #AgCu05 (Fig. 9a) and the “mixed” Ag and Cu NPs (Fig. 9b) after the DSC analysis. The eutectic mixture (Ag)+(Cu) has been obtained in both cases.

Fig. 10 The melting temperature dependence of the Ag-Cu eutectic nanoalloy and elemental Ag and Cu, as a function of nanoparticle size calculated by the CALPHAD method and/or the

LLM model (Eq.(1)). For a comparison, the experimental data on Ag-Cu bimetallic NPs: (+) present work; (*²⁸); Ag (■⁴², ▼⁴³, ▲⁴⁴) and Cu (●²⁸) metal NPs are also shown.

Fig. 11 A linear dependence of the melting temperature vs. inverse particle radius for the Ag-Cu eutectic nanoalloys together with calculated points (Δ). For a comparison, the experimental data on Ag-Cu bimetallic NPs: (+) present work; (*²⁸) are also shown.

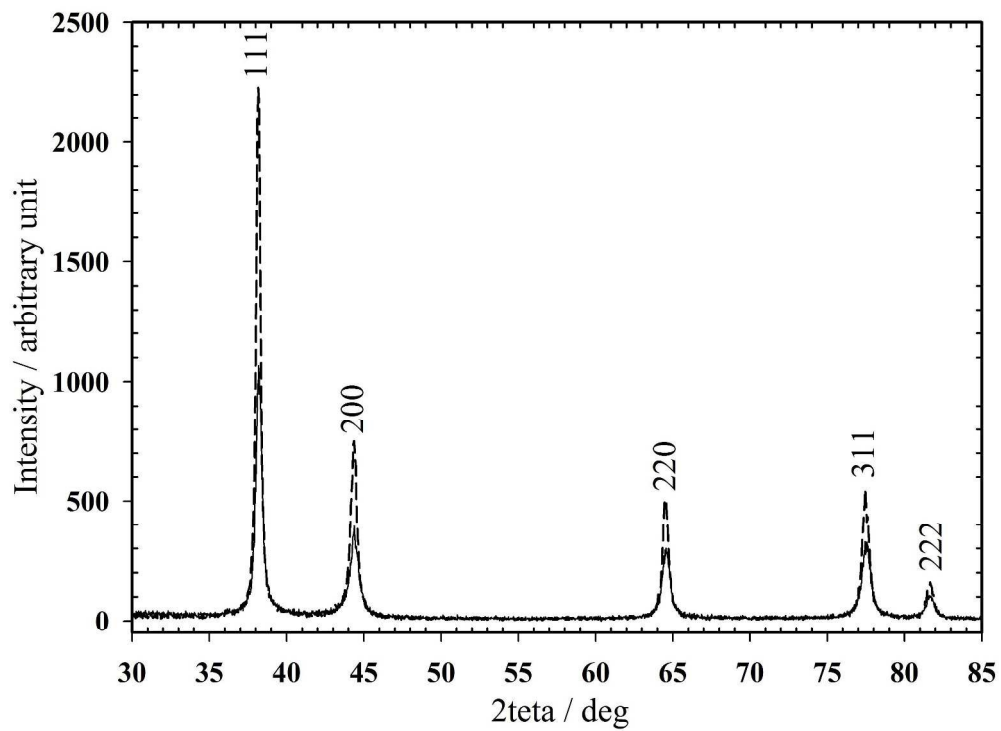


Fig 1

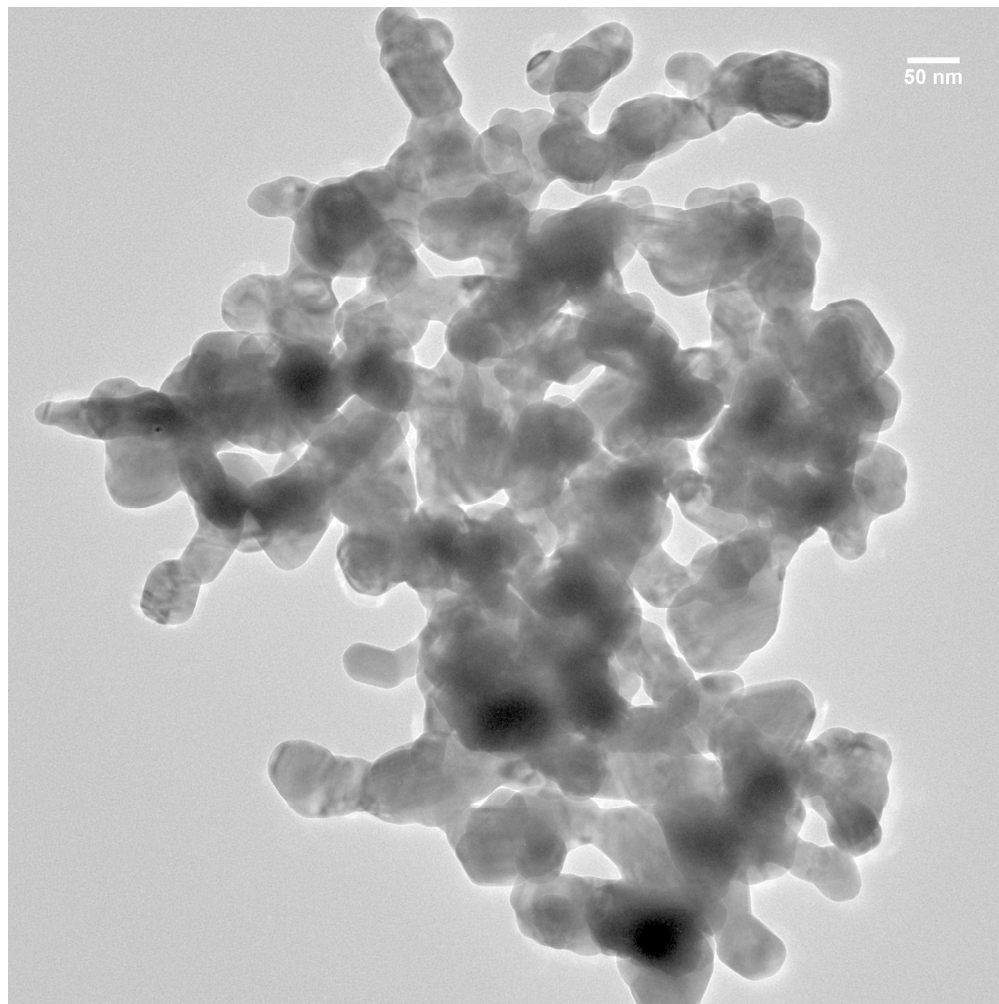


Fig 2
722x722mm (72 x 72 DPI)

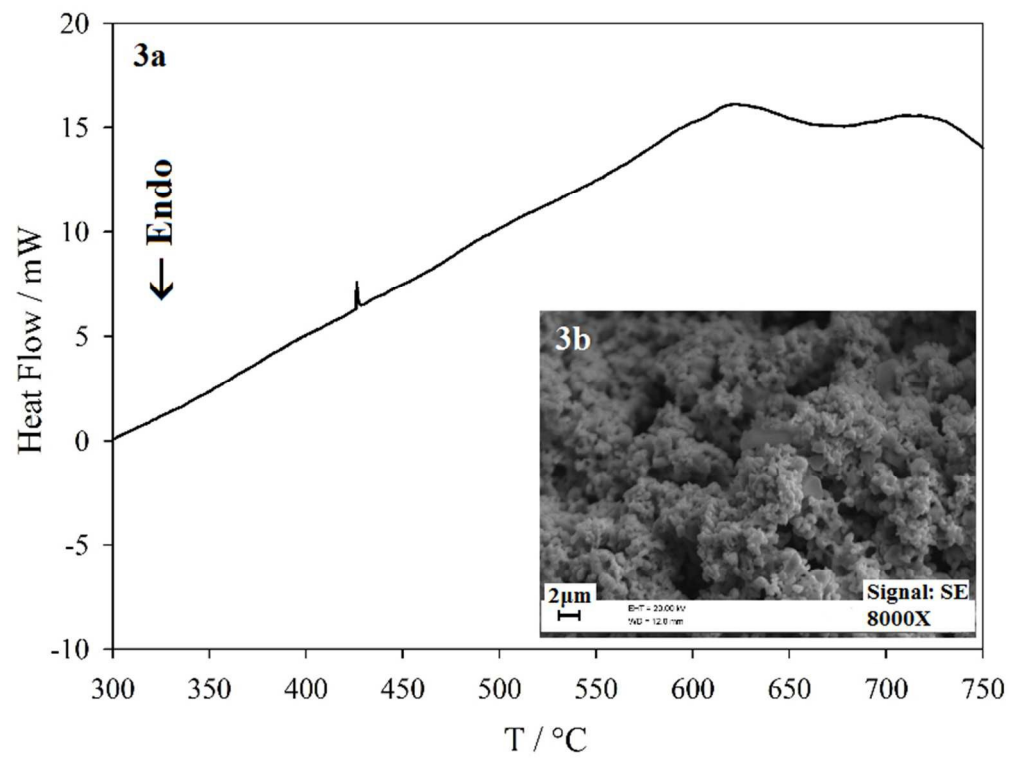


Fig 3
220x165mm (96 x 96 DPI)

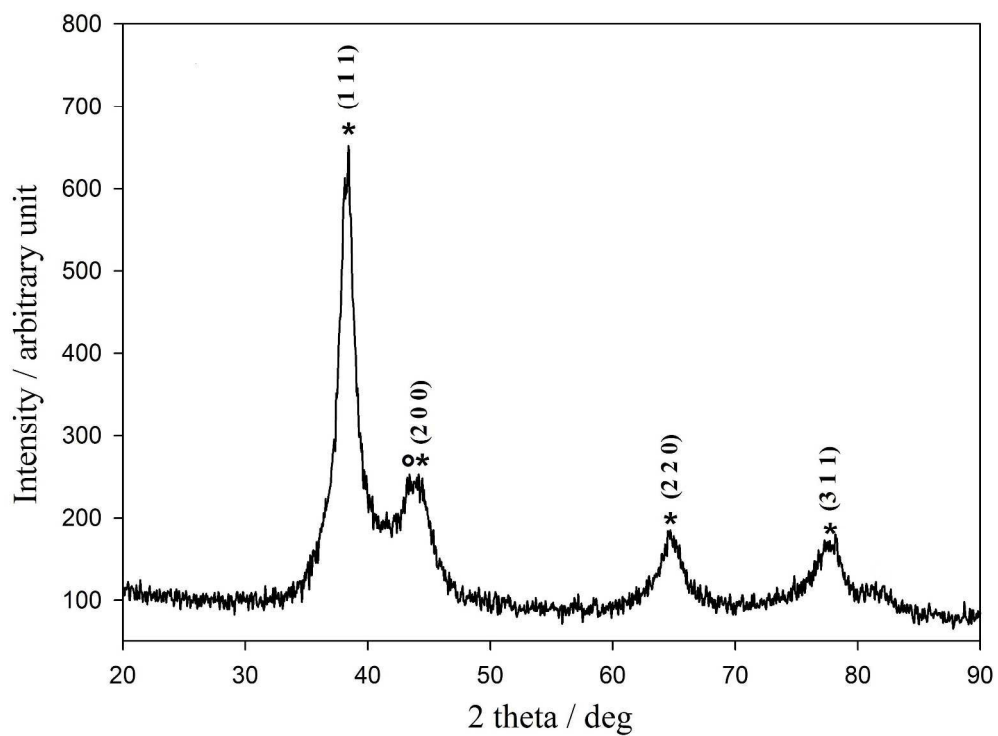


Fig 4
912x672mm (96 x 96 DPI)

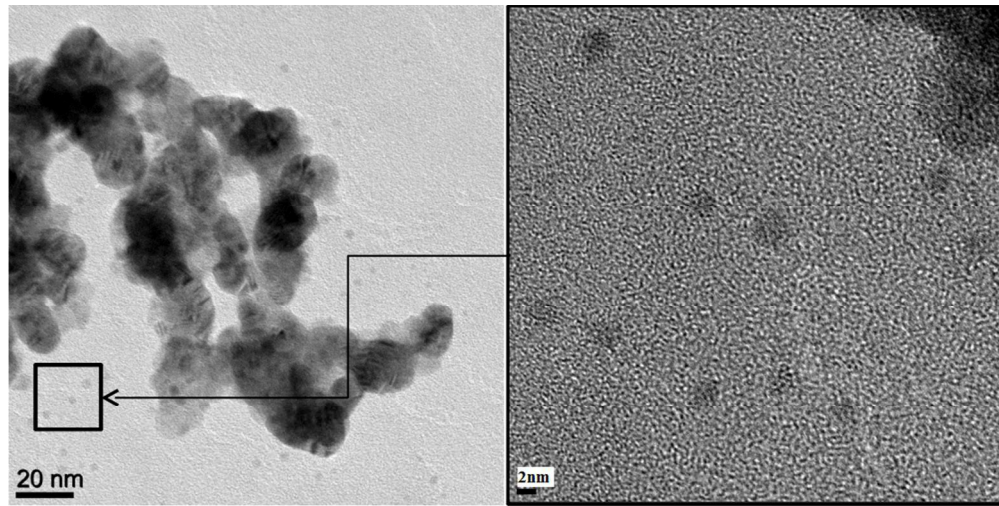


Fig 5
291x146mm (96 x 96 DPI)

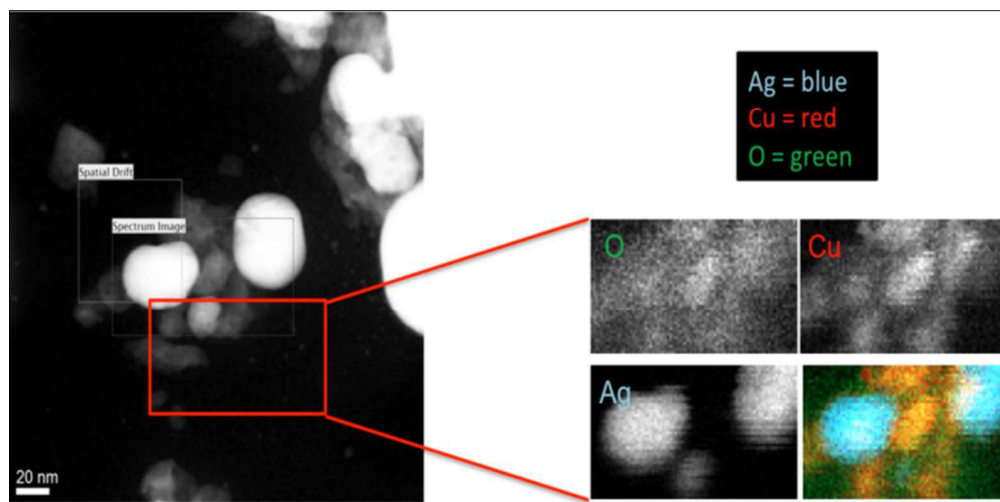


Fig 6
215x107mm (96 x 96 DPI)

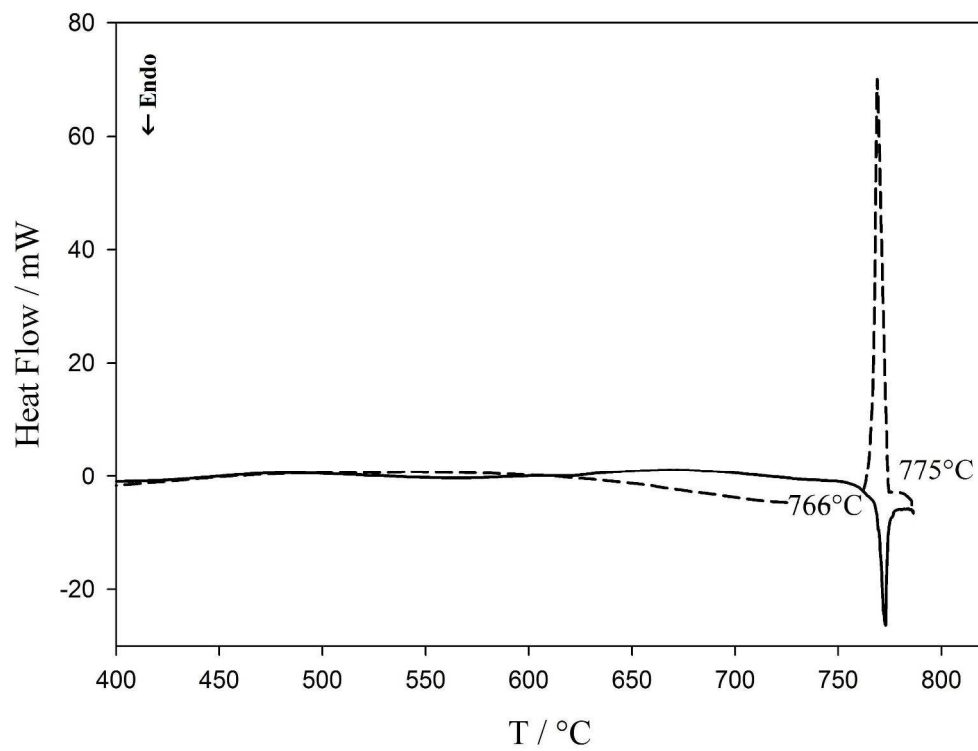


Fig 7

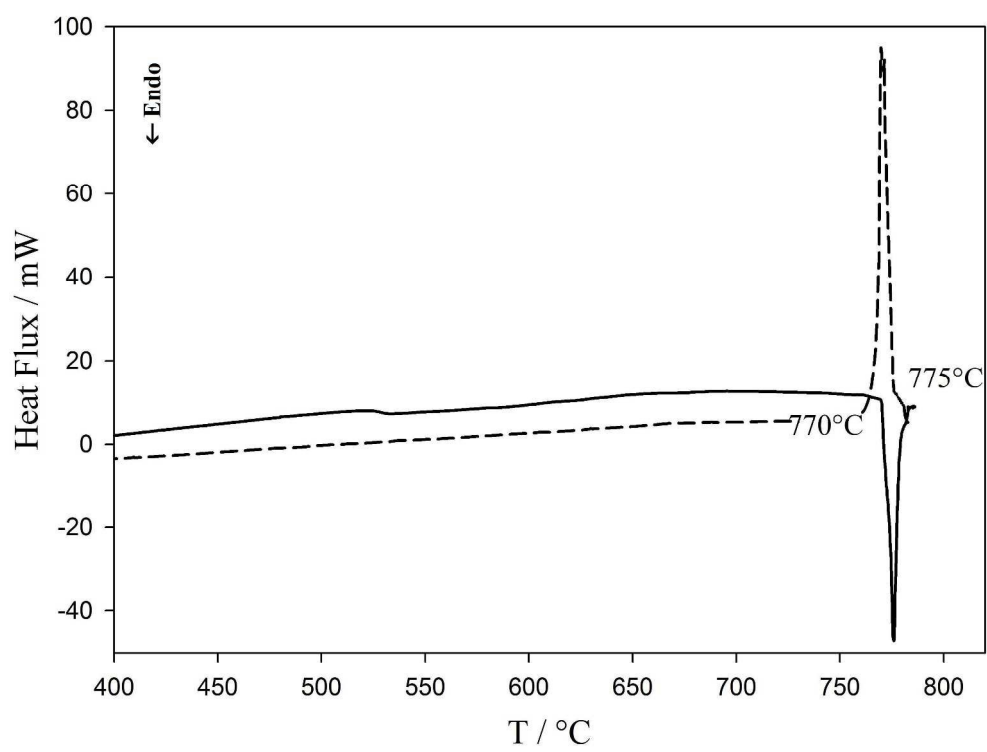


Fig 8

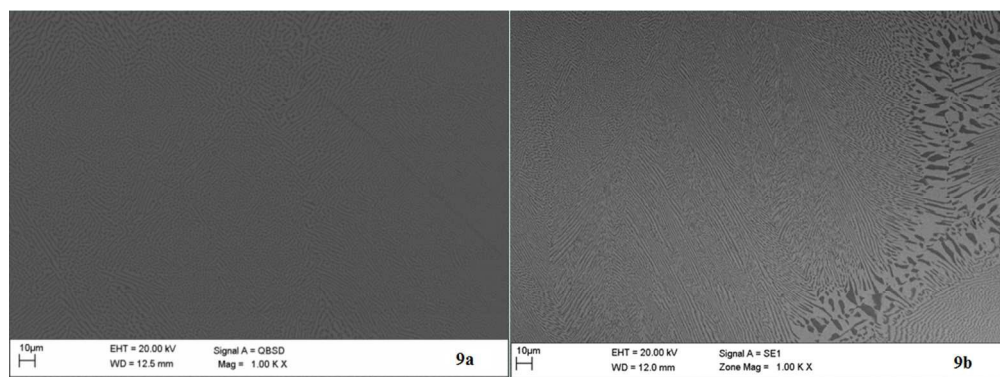


Fig 9
312x117mm (96 x 96 DPI)

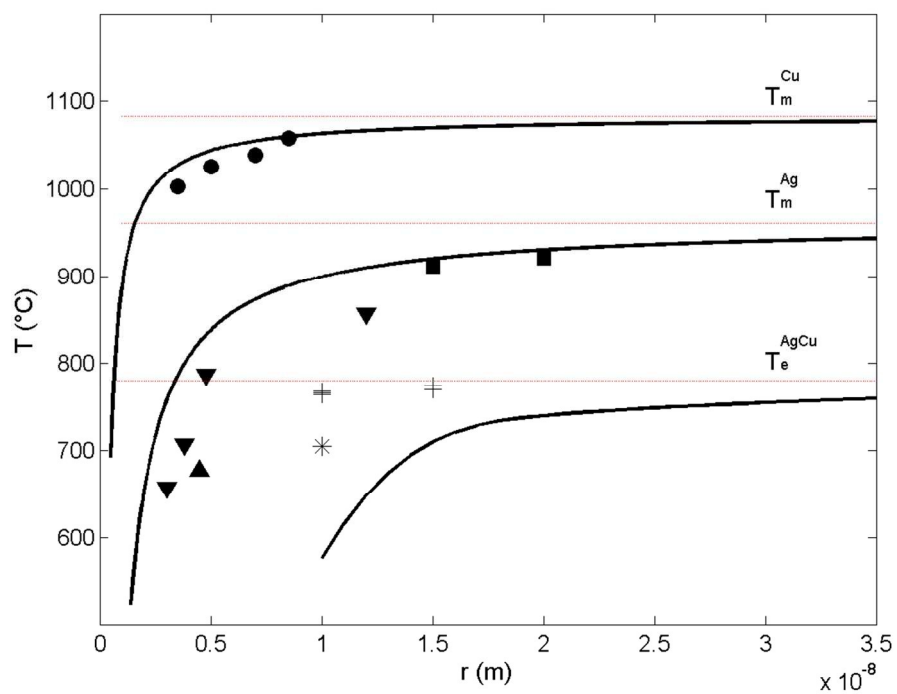


Fig 10
203x152mm (150 x 150 DPI)

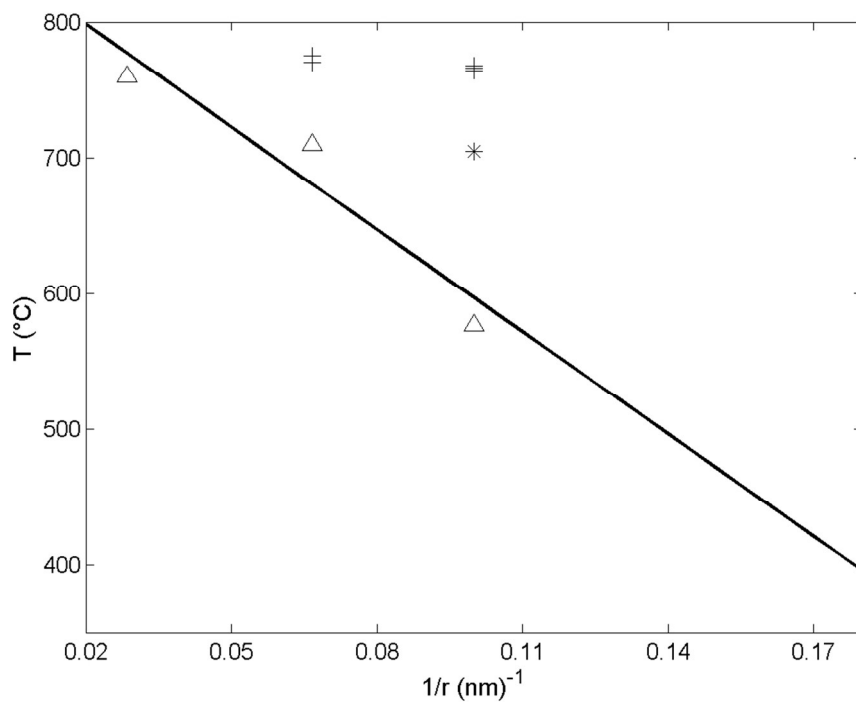


Fig 11
203x152mm (150 x 150 DPI)